JHEP

Published for SISSA by Springer

Received: July 8, 2022
Revised: November 25, 2022
Accepted: November 28, 2022
Published: December 29, 2022

Top-philic dark matter in a hybrid KSVZ axion framework

Anupam Ghosh,[a,b] **Partha Konar**[a] **and Rishav Roshan**[c]

[a] *Theoretical Physics Division, Physical Research Laboratory, Shree Pannalal Patel Marg, Ahmedabad 380009, Gujarat, India*
[b] *Discipline of Physics, Indian Institute of Technology, Palaj, Gandhinagar 382424, Gujarat, India*
[c] *Department of Physics, Kyungpook National University, Daegu, 41566, Korea*

E-mail: anupam@prl.res.in, konar@prl.res.in, rishav.roshan@gmail.com

Abstract: We explore a two-component dark matter scenario in an extended Kim-Shifman-Vainshtein-Zakharov (KSVZ) axion framework. This hybrid setup incorporates an extra $SU(2)_L$ complex singlet scalar whose lightest component plays the role of one of the dark matter, while the QCD axion of the KSVZ model acts as a second dark matter candidate. In this work, we focus on accentuating the role of vector-like quark that naturally emerges in the KSVZ extension on the dark matter and collider phenomenology. Here, we demonstrate that the presence of this colored particle can significantly affect the allowed dark matter parameter space of the scalar dark matter by opening up additional co-annihilation as well as the direct detection channels. Moreover, the interaction between the color particle with the top quark and scalar dark matter provides a unique topology to generate a boosted-top pair with considerable missing transverse momentum at the LHC. Using jet substructure variables and multivariate analysis, here we show that one can already exclude a vast region of parameter space with 139 fb^{-1} integrated luminosity at 14 TeV LHC.

Keywords: Dark Matter at Colliders, Jets and Jet Substructure

ArXiv ePrint: 2207.00487

https://doi.org/10.1007/JHEP12(2022)167

JHEP12(2022)167

Contents

JHEP12(2022)167

1 Introduction

The Standard Model (SM) of fundamental particles is one of the outstanding achievements of modern-day physics, which has been experimentally verified at many frontiers. Ever since the discovery of the Higgs boson [1, 2], the last missing piece of SM, the particle physics community is eagerly scrutinizing collider data to witness if nature can offer a glimmer of hope in the ongoing hunt for new physics. Physics beyond the SM (BSM) is envisaged as inevitable since SM still fails to account for various issues to give us a fully coherent description of nature. Some of the principal concerns are related to the Strong CP problem [3, 4], the existence of the dark matter (DM) [5, 6] in the Universe, non-zero but minuscule neutrino masses [7–9], matter-antimatter asymmetry of the Universe [10, 11] etc. The incapability of the SM in explaining these issues motivates us to look at possible extensions accommodating these aspects.

Different celestial observational evidence [5, 6] at diverse length scales suggests the existence of a non-baryonic, non-luminous, gravitationally interacting form of matter in the Universe, which is popularly known as the *dark matter*. Precision measurement of anisotropies in cosmic microwave background radiation (CMBR) in Wilkinson Microwave Anisotropy Probe (WMAP) [12] and PLANCK [13] played a crucial role in providing us with a valuable estimate of the present abundance of DM relic density. Despite these shreds of evidence in different formats, the particle nature of the DM is still obscured from us. Different

DM paradigms exist in the literature attempting to explain the DM's particle nature. Some of the most popular ones are weakly interacting massive particles (WIMP) [14–21], feebly interacting massive particle (FIMP) [22–29], asymmetric dark matter models [30, 31], models with axion or axion-like particle (ALP) DM [32–35] etc. Although these models can explain the DM relic density of the Universe, their parameter spaces are restricted from different experimental searches. For instance, WIMP dark matter is severely constrained from null detection of the DM in the collider searches [36, 37] as well as the direct [38–41] and indirect [42–44] search experiments.

Interestingly such a null outcome in experimental searches can instead be an indication of a much richer dark sector, and the dark sector can possibly be composed of more than one component of DM. In recent times, there have been several proposals for a multicomponent dark matter [45–58] where the dark sector is made up of different DM components. For example, one can think of a scenario with WIMP-WIMP [45–49] dark matter candidates, WIMP-FIMP [50–52] dark matter candidates, FIMP-FIMP [53, 54] dark matter candidates, WIMP-axion [55, 56] dark matter candidates, etc. In the present work, we aim to explore one such scenario where the dark sector constitutes a WIMP-type dark matter, and the QCD axion plays the role of a second dark matter.

The minimal extension of the SM that can accommodate a WIMP dark matter is its extension by a scalar singlet field with a Higgs portal interaction [59–61]. Here, the DM is assumed to have an odd charge under a discrete unbroken Z_2 symmetry that guarantees its stability. This particular DM scenario is in tension with direct search experiments. The recent direct detection data from the XENON1T experiment [41] has nearly ruled out the DM with mass below 1 TeV [46, 48, 62] apart from the near Higgs resonance region. Reviving this sub-TeV parameter space of the scalar singlet DM could be an exciting undertaking since it can open the possibility of its testing at different frontiers like direct, indirect, and collider searches. One possible way to revive this sub-TeV parameter space is to embed this scalar DM in a two-component framework [46, 48]. With various extensions of two-component DM with a scalar singlet already in place, an interesting exercise could explore the insertion of a scalar singlet in a QCD axion DM framework, as it can enlarge the scalar singlet DM parameter space and can also provide rich collider phenomenology.

Extension of the SM with a global Peccei-Quinn (PQ) symmetry [3, 4] provides solutions for two of the critical issues discussed above in one go, i.e., the *Strong CP problem* and the existence of *dark matter*. This global symmetry is expected to be broken at a scale much larger than the Electroweak (EW) scale. The breaking of $\mathrm{U}(1)_{\mathrm{PQ}}$ predicts a pseudo-Goldstone particle, popularly known as the *QCD axion*, that is not absolutely stable but can have a lifetime much greater than the age of the Universe [32–35] to play the role of DM. There are primarily three different QCD axion models that can simultaneously explain the presence of the DM in the Universe and solve the Strong CP problem. The (i) Peccei-Quinn-Weinberg-Wilczek (PQWW) [3, 63, 64] model introduces an additional singlet scalar that also obtains a non-zero vacuum expectation value (vev) at the time of EW phase transition. This setup is already ruled out from the experiments. The (ii) Kim-Shifman-Vainshtein-Zakharov (KSVZ) [65, 66] model introduces an extra colored particle together with a complex scalar that breaks the PQ symmetry. Anomaly-free

JHEP12(2022)167

condition is ensured by the introduction of vector-like quarks (VLQ). Finally, the (iii) Dine-Fischler-Srednicki-Zhitnitsky (DFSZ) [67, 68] model incorporates an additional Higgs field apart from the PQ breaking scalar. It is also interesting to point out that the breaking of PQ symmetry in these models also leaves a remnant Z_2 symmetry that remains intact. If such a setup is extended with an extra particle that also carries a non-trivial Z_2, then this unbroken symmetry can naturally ensure its stability. This motivates us to study two-component DM scenarios in these models.

In the present work, we aim to explore a hybrid KSVZ scenario, where an extra complex scalar singlet extends the particle spectrum of the KSVZ setup in addition to the usual complex scalar that breaks the PQ symmetry. As mentioned above, the breaking of $\mathrm{U}(1)_{\mathrm{PQ}}$ symmetry in the KSVZ construction leaves remnant Z_2 symmetry which remains unbroken throughout, and the VLQ present in the setup carries an odd charge under it. If the model is extended by a complex scalar that also holds a non-trivial charge under the same Z_2, the lightest component of the scalar can play the role of the second dark matter, making the dark sector two-component.

Note that our setup is similar to the one considered in [55, 56] but with some crucial differences. For example, the present framework considers an up-type VLQ rather than a down-type VLQ, and it opens up a non-trivial possibility in collider analysis. Current construction also aims to explore the possibility of DM effective annihilations (including the DM co-annihilation with the vector-like quark as well as the annihilation of the vector-like quark to the SM particles) to the SM particles in obtaining the correct relic density of the scalar (WIMP) DM. Next, both [55, 56] did not consider the VLQ's contribution to the DM-nucleon spin-independent scattering, which can play a crucial role in the DM phenomenology of WIMP dark matter. This feature of DM effective annihilation to the SM particles, as well as the role of the VLQ in the tree level spin-independent DM-nucleon scattering, was also discussed in [62]. Ref. [62] featured a VLQ doublet and VLQ singlet fermions, unlike ours with a singlet VLQ which naturally occurs in a KSVZ scenario. We also want to emphasize that, although [55, 56, 62] featured some discussions on the collider aspect of this kind of setup, none of them explored it in detail. In the present work, we also perform an exhaustive colliders analysis and aim to find out the relevant parameter space, which would not only validate the dark matter phenomenology but also be consistent with the collider searches.

The paper is organized as follows. We introduce our model in section 2 where the particle spectrum together with their charges under different symmetry groups have been discussed. Various theoretical and experimental constraints in our model are presented in section 3. In section 4 we discuss the dark matter phenomenology of the model. The collider analysis and the result based on multivariate analysis are presented in section 5. Finally, we summarize our findings in section 6.

2 The model

As stated in the introduction, the present work aims to study dark matter and collider phenomenology in a hybrid KSVZ framework of QCD axion. As is well known, the vanilla

JHEP12(2022)167

	η	S	Ψ
$\mathrm{SU}(3)_C$	1	1	3
$\mathrm{SU}(2)_L$	1	1	1
$\mathrm{U}(1)_Y$	0	0	2/3
$\mathrm{U}(1)_{\mathrm{PQ}}$	2	1	1

Table 1. Particle contents and their respective charge assignments under different symmetry groups.

KSVZ model requires a complex scalar singlet η that breaks a global symmetry, popularly known as $\mathrm{U}(1)_{\mathrm{PQ}}$. In addition, this model also demands a $\mathrm{SU}(2)_L$ singlet colored fermion Ψ with a $+1$ unit of $\mathrm{U}(1)_{\mathrm{PQ}}$ charge. This extra quark is vector-like and hence does not introduce any chiral anomaly. In addition, the hybrid KSVZ model also introduces an additional complex singlet scalar S charged under the $\mathrm{U}(1)_{\mathrm{PQ}}$. The BSM fermion and scalar content of the model and their respective charges are listed in table 1. The most general renormalizable and gauge-invariant Lagrangian for the present setup can be written as,

$$-\mathcal{L}^{\mathrm{VLQ}} = f_i S\overline{\Psi}_L u_{iR} + f_\Psi \eta \overline{\Psi}_L \Psi_R + h.c., \tag{2.1}$$

where, u_R represents right-handed up-type quarks in the SM with $i = u, c, t$. Here, L and R denote left- and right-handed projections. Note that the hypercharge of the newly introduced VLQ depends on its interaction with SM quarks. The relevance of introducing an up-type VLQ in this setup will be clear once we discuss the DM and collider phenomenologies in sections 4 and 5 respectively.

Moving on to the scalar part of the Lagrangian, the most general renormalizable scalar potential of our model, $V(H, \eta, S)$ can be written as,

$$\begin{aligned} V(H,\eta,S) = {} & \lambda_H(|H|^2 - v_H^2/2)^2 + \lambda_\eta(|\eta|^2 - F_a^2/2)^2 + \lambda_{\eta H}(|H|^2 - v_H^2/2)(|\eta|^2 - F_a^2/2) \\ & + \mu_S^2|S|^2 + \lambda_S|S|^4 + \lambda_{SH}|H|^2|S|^2 + \lambda_{S\eta}|\eta|^2|S|^2 + [\epsilon_S \eta^* S^2 + h.c]. \end{aligned} \tag{2.2}$$

After the breaking of both $\mathrm{U}(1)_{\mathrm{PQ}}$ and the SM gauge symmetry, the different scalars involved in the present setup take the following form,

$$H = \begin{pmatrix} 0 \\ \frac{1}{\sqrt{2}}(v_H + h_0) \end{pmatrix}, \quad \eta = e^{\frac{ia}{F_a}} \frac{(F_a + \sigma_0)}{\sqrt{2}}, \quad S = \frac{S_1 + iS_2}{\sqrt{2}}, \tag{2.3}$$

where v_H denotes the vacuum expectation value (vev) of H obtained after the electroweak symmetry breaking (EWSB) and F_a represents the $\mathrm{U}(1)_{\mathrm{PQ}}$ breaking scale. It is to be noted that, after the breaking of both symmetries, a non-zero $h_0 - \sigma_0$ mixing leads to the following mass terms:

$$M^2 \equiv \begin{pmatrix} 2v_H^2\lambda_H & F_a v_H \lambda_{\eta H} \\ F_a v_H \lambda_{\eta H} & 2F_a^2 \lambda_\eta \end{pmatrix}. \tag{2.4}$$

The mass matrix can be diagonalised using

$$\begin{pmatrix} h_0 \\ \sigma_0 \end{pmatrix} = \begin{pmatrix} \cos\theta_m & \sin\theta_m \\ -\sin\theta_m & \cos\theta_m \end{pmatrix} \begin{pmatrix} h \\ \sigma \end{pmatrix} \tag{2.5}$$

JHEP12(2022)167

where the mixing angle is given by,

$$\tan(2\theta_m) = \frac{F_a v \lambda_{\eta H}}{F_a^2 \lambda_\eta - v^2 \lambda_H}\,. \tag{2.6}$$

Finally, after diagonalization, the physical masses of the h and σ are given as,

$$M^2_{h,\sigma} = (\lambda_H v^2 + \lambda_\eta F_a^2) \pm \sqrt{(\lambda_H v^2 - \lambda_\eta F_a^2)^2 + F_a^2 v^2 \lambda^2_{\eta H}}\,. \tag{2.7}$$

Next, as an artifact of two different symmetry breakings, the masses of the different components of the S can be expressed as,

$$M^2_{S_{1,2}} = \frac{1}{2}\left(2\mu_S^2 + v_H^2 \lambda_{SH} + F_a^2 \lambda_{S\eta} \mp 2\sqrt{2}\epsilon_s F_a\right). \tag{2.8}$$

Notice that the presence of the term proportional to ϵ_S in eq. (2.2) plays a crucial role in generating the mass splitting among the components of S. Subsequently, the mass of the VLQ is given as,

$$M_\Psi = f_\Psi \frac{F_a}{\sqrt{2}}. \tag{2.9}$$

At this stage, it is interesting to point out that, even after the breaking of both the symmetries, there still exists a remnant Z_2 symmetry under which both the Lagrangian as well as the scalar potential remains invariant. This remnant Z_2 can remain intact if S does not acquire a non-zero vev. Under such a scenario, the lightest neutral component of S can provide a vital DM candidate.

Finally, the setup also contains a pseudo-Nambu Goldstone boson a, associated with scalar η, popularly known as *axion*. The axion obtains a mass as a result of non-perturbative QCD effects given as [32, 34],

$$m_a \simeq 0.6 \text{ meV} \times \left(\frac{10^{10} \text{ GeV}}{F_a}\right). \tag{2.10}$$

Note that a suitable choice of decay constant F_a can adjust the fraction of which QCD axion can contribute toward the relic density of the dark matter. That makes the preset setup a tunable two-component dark matter scenario. The role of QCD axion as a DM candidate and its constraints are elaborated in section 4. Now with the knowledge of all the particles and their interactions in this hybrid KSVZ setup, we are in a position to list the set of independent parameters important for the dark matter and collider phenomenology:

$$\{M_\Psi, M_{S_1}, M_{S_2}, M_\sigma, F_a, \lambda_{SH}, \lambda_{S\eta}, f_i\}.$$

JHEP12(2022)167

3 Experimental and theoretical constraints

The extended KSVZ model under consideration is subjected to various theoretical as well as experimental constraints. In this section, we summarize all the relevant ones.

- **Stability and perturbativity.** The scalar sector is extended over the vanilla model. Hence, different scalars in the present setup can help stabilize the electroweak vacuum. The stability of the electroweak vacuum also demands that the scalar potential should be bounded from below in all the field directions of the field space. On the other hand, a perturbative theory demands that the model parameters should obey:

$$|\lambda_i| < 4\pi \text{ and } |g_i|, |y|, |f_i| < \sqrt{4\pi}, \tag{3.1}$$

  where g_i and y are the SM gauge and Yukawa couplings, whereas f_i are Yukawa couplings involving different BSM fields, respectively.

- **Relic density, direct and indirect detection of DM.** For any dark matter model, it is essential to satisfy the observed abundance of DM relics from the precision measurement in the Planck experiment [69],

$$\Omega_{\rm DM}h^2 = 0.120 \pm 0.001. \tag{3.2}$$

  Apart from DM relic density, the DM-nucleon scattering cross-section is also constrained by various direct search experiments like LUX [38], PandaX-II [39, 40], and XEXON1T [41]. Finally, the DM annihilation to the SM particles are also subjected to the constraints coming from the indirect search experiments like PAMELA [42], Fermi-LAT [44], MAGIC [43] etc. Nonetheless, in all these cases, one also needs to take care of the multi-component nature of DM in our extended scenario, which is further discussed in section 4.

- **Flavor constraints.** The Yukawa interactions of the complex singlet scalar S with VLQ and the SM right-handed quarks like u and c in the present setup can contribute towards the $D^0 - \bar{D}^0$ mixing [70]. The measured value of the D-meson mass splitting significantly constrained this mixing. The Feynmann diagrams that contribute to this mixing are shown in figure 15; each diagram has four possible configurations with a total of sixteen diagrams. Effective operator contributing to this mixing in the present setup can be expressed as

$$\mathcal{L}_{\rm eff} = \frac{\tilde{z}}{M_\Psi^2}\bar{u}_R^\alpha \gamma^\mu c_R^\alpha \bar{u}_R^\beta \gamma_\mu c_R^\beta, \tag{3.3}$$

  where

$$\tilde{z} = -\frac{f_u^2 f_c^2}{96\pi^2}[g_\psi(M_{S_1}^2/M_\Psi^2) + g_\psi(M_{S_2}^2/M_\Psi^2) - 2g_\psi(M_{S_1}M_{S_2}/M_\Psi^2)]. \tag{3.4}$$

  Here $g_\Psi(x) = 24x f_6(x) + 12\tilde{f}_6(x)$ where the expressions of f_6 and $\tilde{f}_6$ can be found in [71]. The measurement of the D-meson mass splitting demands $|\tilde{z}| \lesssim 5.7 \times 10^{-7}(M_\Psi/\text{TeV})^2$ [70, 71]

JHEP12(2022)167

- **LHC diphoton searches.** As a result of mixing between h and σ, all the tree level interactions with the SM Higgs get modified. In such a case, the signal strength in the di-photon channel takes a form:

$$\mu_{\gamma\gamma} = c_\theta^2 \frac{BR_{h\to\gamma\gamma}}{BR^{\rm SM}_{h\to\gamma\gamma}} \simeq c_\theta^2 \frac{\Gamma_{h\to\gamma\gamma}}{\Gamma^{\rm SM}_{h\to\gamma\gamma}}. \tag{3.5}$$

  LHC sets a limit on this new mixing angle as $|\sin\theta| \leq 0.36$ [72].

- **Invisible Higgs decay.** Involvement of the new interactions of SM Higgs with various BSM particles in the present setup can lead to its new decay modes if kinematically allowed. These extra decays of Higgs can contribute toward invisible Higgs decay. In such a situation, we need to employ the bound on the invisible Higgs decay width as [73]:

$$Br(h \to \text{Invisible}) \equiv \frac{\Gamma(\text{h} \to \text{Invisible})}{\Gamma(\text{h} \to \text{SM}) + \Gamma(\text{h} \to \text{Invisible})} < 0.11. \tag{3.6a}$$

  In the case of light DM, the Higgs can decay to a pair of it when kinematically allowed. However, in our present analysis, we primarily focus on the parameter space where $m_i > \frac{m_h}{2}$ so the above constraint is not applicable.

- **Direct collider constraints.** Due to the presence of colored vector-like quarks, the present model is subjected to various collider constraints. Being non-trivially charged under the $\text{U}(1)_{\text{PQ}}$ allows the VLQ to couple with the complex scalar and the SM up type quarks. If kinematically allowed, the heavier states can always decay into the DM and an SM quark. Therefore a generic collider signature of this model contains a considerable amount of missing (transverse) energy from the escape of final DM particles from detection at the detector.

  Vector-like fermion can be pair produced through electroweak interaction performed at CERN's Large Electron Positron Collider (LEP):

$$e^+e^- \to \gamma^*, Z \to \Psi\bar{\Psi} \tag{3.7}$$

  The interaction between vector-like fermion, light SM quarks, and the DM can lead to the decay of Ψ to a light quark associated with DM at LEP if kinematically allowed. The reinterpreted LEPII results of squark search [74, 75] exclude the mass of Ψ up to 100 GeV. Such constraint is incorporated in our final exclusion plots. Please follow the brown region in figure 10. Similar searches were also carried out at the LHC. In a recent ATLAS search, the vector-like mediator is searched while it decays into an invisible particle and light quark up (charm) when the mass difference between the mediator and DM is less than the top quark mass. The green region in figure 10 is excluded from the reinterpreted result [74] of the ATLAS search [76] for multijet (2–6 jets) plus missing transverse momentum at center-of-mass (CM) energy $\sqrt{s} = 8$ TeV with an integrated luminosity of 20.3 fb^{-1}. Exploring a larger mass difference between the mediator and DM candidate, top-antitop plus missing transverse momentum signal

JHEP12(2022)167

has been extensively studied by both CMS and ATLAS collaborations, particularly superpartners searches of the top quark [77–85] and some dedicated dark matter searches [37]. The vector-like mediator can be pair produced at the LHC mainly through strong interaction and then decay into an up-type quark and invisible particle. So, the search for a top pair along with the missing transverse momentum signature by ATLAS and CMS can be reinterpreted to exclude some of the parameter spaces of this model. The CMS analysis [85] is reinterpreted in ref. [86] at 13 TeV LHC for an integrated luminosity of 35.9 fb^{-1}, assuming vector-like mediator decay with 100% branching fraction into the top and invisible particle. In their analysis, the signal consists of two oppositely charged isolated leptons from leptonic decays of both top and anti-top. The signal also consists of at least two hard jets; one of them is b-tagged and a large missing transverse momentum. The olive region in figure 10 is the exclusion region (2σ) obtained from this analysis.

The existing LHC search relies on finding the top pair based on two hard leptons and a b-tagged jet. It is evident that the sensitivity of such detection deteriorates when these tops are boosted, especially while decaying from a heavy mother particle. We propose an alternative search strategy in this work by recognizing these boosted double top jets with a large missing transverse energy signature using jet substructure variables and multivariate analysis. We are examining the spectrum where the mass difference between vector-like mediator and DM is larger than the mass of the top quark such that on-shell decay into the top is possible. Our search strategy helps to explore the significant parameter space of this model that gives observed relic density of DM and also allowed from the direct-detection experiment with the current luminosity of the LHC.

4 Dark matter phenomenology

In this section, we aim to elaborate on the DM phenomenology of the model under consideration. As discussed earlier, the setup is a hybrid of the KSVZ model that includes an extra complex scalar (S) whose lightest component (S_1) plays the role of one of the DM while the part of the second DM is played by the QCD axion of the KSVZ setup. The involvement of the two DMs in this extended KSVZ scenario makes the layout a two-component DM system. Besides the QCD axion, the KSVZ setup naturally demands a presence of an extra colored fermionic $\text{SU}(2)_L$ singlet. This fermion plays a non-trivial role in the DM phenomenology and the collider searches of the DM as it talks directly to it through the Yukawa interaction given in eq. (2.1). Next, we discuss the DM phenomenology of both the DM candidates of the present model.

4.1 Relic density and DM detection

Apart from providing a solution to the *strong CP problem*, another interesting consequence of introducing a PQ symmetry is the emergence of the Nambu Goldstone boson, popularly known as *axion*. If the breaking scale (F_a) of the PQ symmetry is chosen appropriately, the resulting axion can be light as well as stable. This QCD axion can be an excellent DM

JHEP12(2022)167

candidate in such a scenario. Axions can be produced non-thermally as a result of the misalignment mechanism. Here, the axion field begins to coherently oscillate around the minimum of the PQ vacuum when its mass becomes comparable to the Hubble parameter. This coherent oscillation of the axion field behaves like a cold matter in the Universe. The relic density of the axion in such a case is approximately given by [55, 56, 87],

$$\Omega_a h^2 \simeq 0.18\, \theta_a^2 \left(\frac{F_a}{10^{12}\text{GeV}}\right)^{1.19}. \tag{4.1}$$

Here, θ_a represents the initial misalignment angle of the axion.

For the case of the scalar DM, we consider the mass hierarchy $M_{S_2} > M_{S_1}$ such that the lightest scalar component represents the second DM candidate. Its interactions with the SM Higgs and the VLQ keep it in equilibrium with the thermal bath in the early Universe. As the temperature of the Universe drops below the DM mass, its production from the thermal bath stops while its annihilation of the SM particle continues. Once the Universe's expansion rate becomes larger than the interaction rate of the DM, its annihilation to the SM bath also stops, and its abundance freezes out. DM can annihilate to the SM particles through: (a) its contact interactions, (b) Higgs-mediated channels[1] and (c) VLQ mediated channels (as a result of Yukawa interaction given in eq. (2.1)). The presence of the Yukawa interaction also allows the DM to co-annihilate if the mass-splitting between the DM and newly introduced quark is sufficiently small. Note that as the VLQ and S_2 share the same Z_2 charge similar to the DM, their annihilations would also be important for evaluating the effective annihilation cross-section. In appendix A, we present all the important annihilation and co-annihilation channels of the DM that are crucial in determining its final relic abundance.[2] Once all the important annihilation and co-annihilation channels are identified, one can use them to determine the final relic density of the DM, which can be expressed as [60],

$$\Omega_{S_1} h^2 = \frac{1.09 \times 10^9\ \text{GeV}^{-1}}{g_*^{1/2}\ M_{Pl}} \frac{1}{J(x_f)}, \tag{4.2}$$

where $J(x_f)$ is given by,

$$J(x_f) = \int_{x_f}^{\infty} \frac{\langle\sigma|v|\rangle_{\text{eff}}}{x^2}\ \text{dx}. \tag{4.3}$$

$\langle\sigma|v|\rangle_{\text{eff}}$ in eq. (4.3) is the effective thermal average DM annihilation cross-sections including contributions from the co-annihilations and is given by,

$$\begin{aligned}\langle\sigma|v|\rangle_{\text{eff}} = {} & \frac{g_{s_1}^2}{g_{\text{eff}}^2}\sigma(\overline{S_1}S_1) + 2\frac{g_{s_1}g_{s_2}}{g_{\text{eff}}^2}\sigma(\overline{S_1}S_2)(1+\Delta_{12})^{3/2}\ \exp[-x\Delta_{12}] + 2\frac{g_{s_1}g_{\Psi}}{g_{\text{eff}}^2}\sigma(\overline{S_1}\Psi)(1+\Delta_{\Psi})^{3/2} \\ & \exp[-x\Delta_{\Psi}] + \frac{g_{S_2}^2}{g_{\text{eff}}^2}\sigma(\overline{S_2}S_2)(1+\Delta_{12})^3\ \exp[-2x\Delta_{12}] + \frac{g_{\Psi}^2}{g_{\text{eff}}^2}\sigma(\overline{\Psi}\Psi)(1+\Delta_{\Psi})^3 \\ & \exp[-2x\Delta_{\Psi}].\end{aligned} \tag{4.4}$$

[1] From eq. (2.7), it is evident that until and unless λ_η is very small, M_σ will remain much heavier than M_h and hence the σ mediated annihilation channels be very much suppressed.

[2] Just for completeness we have also shown the DM annihilation to the axion final states. These annihilations are highly suppressed and do not contribute towards the relic density of scalar dark matter. This is because most of the vertices involved in these annihilation cross-sections are either proportional to $1/F_a$ or $\frac{\sin\theta}{F_a}$ or $\frac{\epsilon_S}{F_a}$ or ϵ_S.

JHEP12(2022)167

In the equation above, g_{s_1}, g_{s_2} and g_Ψ are the spin degrees of freedom for S_1, S_2 and Ψ. Here, $x = \frac{M_{S_1}}{T}$ representing dimensionless parameter with inverse of temperature, while Δ_Ψ and Δ_{12} are two dimensionless parameters qualifying mass splittings from dark scalar candidate:

$$\Delta_\Psi = \frac{M_\Psi - M_{S_1}}{M_{S_1}};\ \Delta_{12} = \frac{M_{S_2} - M_{S_1}}{M_{S_1}}. \tag{4.5}$$

The effective degrees of freedom in eq. (4.4) is given by,

$$g_{\text{eff}} = g_{s_1} + g_{s_2}(1+\Delta_{12})^{3/2}\ \exp[-x\Delta_{12}] + g_\Psi(1+\Delta_\Psi)^{3/2}\ \exp[-x\Delta_\Psi]. \tag{4.6}$$

In the following analysis, we first generate the model using FeynRules [88] and then implement it in `micrOMEGAs` -v5 [89] to find the region of parameter space that corresponds to correct relic abundance for our scalar DM candidate in accordance with the relation,

$$\Omega_{\text{T}}h^2 = \Omega_a h^2 + \Omega_{S_1}h^2, \tag{4.7}$$

where $\Omega_{\text{T}}h^2$ corresponds to the total relic density of the DM satisfying PLANCK constraints [69].

Next, the present model is subjected to the constraints coming from the direct search experiments for the dark matter. Experiments like LUX [38], PandaX-II [39, 40] looks for the DM recoil in the DM-nucleon scattering and subsequently provides a bound on the DM-nucleon scattering cross-section. Being a two-component DM system, the direct detection cross-section of the scalar DM should be rescaled as,

$$\sigma^{\text{SI}}_{S_{1,\text{eff}}} = \frac{\Omega_{S_1}}{\Omega_{\text{T}}}\sigma^{\text{SI}}_{S_1} \tag{4.8}$$

As mentioned earlier, due to the direct Yukawa interaction of the scalar DM with the up-quark, two other scattering processes contribute to the direct detection cross-section of the scalar apart from the usual SM Higgs-mediated scattering. In appendix A we listed all the scattering processes of the DM S_1 with the detector nucleon.

Finally, the model is also subjected to the constraints coming from the indirect search experiments. Indirect search experiments looking for an excess of gamma rays can help in probing the WIMP dark matter. DM particles can annihilate and produce SM particles, out of which photons (and also neutrinos), being electromagnetically neutral, have better chances of reaching the detector from the source without getting deflected. Experiments like PAMELA [42], Fermi-LAT [44], MAGIC [43] etc. look for such excess in order to confirm the particle nature of the DM. The present set up being a two-component DM scenario, the indirect detection cross-section of the scalar DM should be rescaled as well,

$$\sigma^{\text{ID}}_{S_{1,\text{eff}}} = \left(\frac{\Omega_{S_1}}{\Omega_{\text{T}}}\right)^2 \sigma^{\text{ID}}_{S_1}. \tag{4.9}$$

At this stage, it is worth commenting on some of the detection possibilities of the axion as a DM candidate. Several ongoing and proposed experiments rely on axion being a DM. All these experiments lean on different detection techniques. For example, ADMX [90]

JHEP12(2022)167

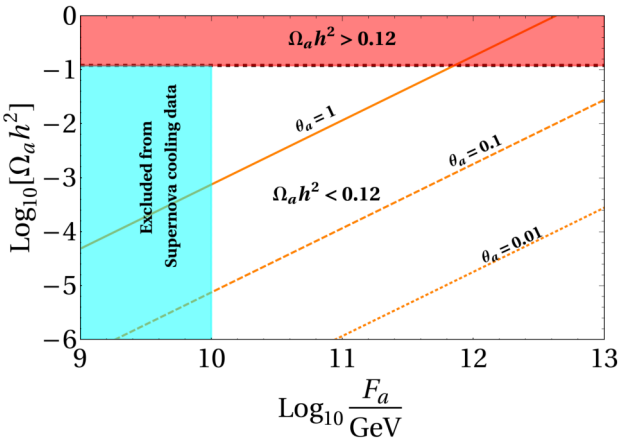

Figure 1. Variation of QCD axion relic density with the decay constant F_a for three different values of misalignment angles: $\theta_a = 1.0$ (solid), $\theta_a = 0.1$ (dashed), and $\theta_a = 0.01$ (dotted). Black thick dashed line corresponds to observed relic $\Omega_{\rm DM}h^2 = 0.12$. The cyan region is disallowed from the Supernova cooling data. The light pink region corresponds to the parameter space where the DM relic density remains overabundant.

searches for DM-photon conversion in the presence of the magnetic field. CASPEr [91] uses nuclear magnetic resonance to hunt for the axion DM; it is known that if the axion exists, it will modify Maxwell's equation. ABRACADABRA [92] utilizes this by using a toroidal magnet to source an effective electric current, and finally, MADMAX [93] is a proposed experiment that uses dielectrics haloscopes.

4.2 Parameter space of hybrid KSVZ axion framework

It is well known that the KSVZ model provides a DM in the form of QCD axion. For this axion to play the role of the DM or contributes sufficiently towards the relic density of the DM, the decay constant F_a should lie in the range,

$$10^{10}\ \text{GeV} \leq F_a \leq 10^{12}\ \text{GeV}. \tag{4.10}$$

The lower bound on F_a comes from the supernova cooling data [94] whereas the upper bound results from the overproduction of the axion or, in other words, the relic density of the axion become overabundant. To understand this, in figure 1 we study the variation of the axion relic density ($\Omega_a h^2$) with the decay constant for three different values of the misalignment angles i.e. $\theta_a = 1.0$ (solid), $\theta_a = 0.1$ (dashed), and $\theta_a = 0.01$ (dotted). The region in cyan is ruled out from the supernova cooling data, whereas the light pink region corresponds to the overproduced DM relic density. As can be seen from figure 1, for $\theta_a = 1.0$ and $F_a \simeq 10^{12}$ GeV, the axion alone can contribute 100% towards the relic density of the dark matter. Finally, the white region corresponds to the parameter space where QCD axion as a DM remains underabundant.

The present setup is an extended version of the KSVZ scenario, which contains an additional DM candidate as a singlet scalar. The presence of this extra DM here demands us to choose a parameter space for axion from figure 1 where the relic density of the axion

JHEP12(2022)167

remains underabundant so that the relic density of the axion together with the scalar can satisfy the Planck limit. For a demonstrative purpose, we fix $F_a = 10^{11}$ GeV and choose the misalignment angle as $\theta_a = 1$ for the rest of the analysis. This choice of F_a and θ_a corresponds to $\Omega_a h^2 = 0.012$. Without losing generality in our analysis, we set a heavier M_σ at 50 TeV (as the setup requires it to be quite heavy). At this stage, we would like to point out that the DM matter couples to σ through $S_1 - S_1 - \sigma$ interaction. This interaction can also help DM to annihilate into the SM particles through scalar mixing. Although these annihilations will have suppression coming from the mass of σ, they might still not be that small as these annihilations are also proportional to the $F_a\lambda_{S\eta}$. With $F_a = 10^{11}$ GeV and not so small value of $\lambda_{S\eta}$, the DM can still have significant annihilation cross-sections and such cross-sections might violate perturbative unitarity [95]. This demands $\lambda_{S\eta}$ to be extremely tiny. For simplicity, we set $\lambda_{S\eta} = 0$ throughout our analysis. Next, for the analysis purpose, we also define a mass-splitting, $\Delta M = M_{S_2} - M_{S_1}$ and consider it to be a free parameter rather than M_{S_2}. It is interesting to point out that once ΔM and F_a are fixed, the parameter ϵ_S automatically gets fixed, as can be seen from eq. (2.8). Before diving into the detailed analysis of the second DM candidate, we will like to mention the set of parameters that are relevant for the analysis of the DM phenomenology of the second DM candidate:

$$\{M_\Psi, M_{S_1}, \Delta M, F_a, \lambda_{SH}, f_i\}.$$

To demonstrate the above discussions, we display the variation of the relic density of S_1 with its mass in all the left panel plots of figure 2. In the right panel, we also exhibit the variation of the effective direct detection cross-section with M_{S_1} for different choices of parameters. In the top left panel of figure 2, we project the importance of the Yukawa coupling f_t while choosing fixed values of $\Delta M = 100$ GeV, $M_\Psi = 500$ GeV and $\lambda_{SH} = 0.01$. It is interesting to point out that for $\lambda_{SH} = 0.01$, the DM does not satisfy the correct relic density in a pure scalar singlet DM scenario. In these plots, we also set both Yukawa couplings $f_u = f_c = 0.01$ to highlight the importance of the top Yukawa coupling f_t for three values of f_t: 0.1 (blue), 0.5 (red) and 1.0 (green). Notice that for $f_t = 0.1$, with the increase in the DM mass, we first observe a resonance dip at $M_{S_1} = M_h/2$,[3] next, a fall is observed at $M_{S_1} = 80$ GeV where the annihilation of the DM to the $W^\pm$ boson opens up after which the relic density increases with the increase in the DM mass ($\langle\sigma v\rangle \propto 1/M_{S_1}$) and again drops at $M_{S_1} = 125$ GeV when the DM starts annihilating into the Higgs boson.[4] Finally, at a larger value of M_{S_1} ($M_{S_1} = 345$ GeV), when the mass difference between M_Ψ and M_{S_1} becomes relatively small, and the effect of DM co-annihilation with the VLQ comes into the picture, and a sharp drop in DM relic density is observed. In this region, although

[3] In a lower DM mass regime, DM annihilating to the three body final states $q\bar{q}g$ can also contribute significantly towards the relic density, where chirality suppression in the lower order process is lifted by final state radiation. We do not consider this three-body final state in our analysis as the entire low mass regime of the DM is already ruled out from the DD searches, as can be seen from the right panels of figure 2.

[4] We would also like to point out that for DM mass $M_{S_1} < M_t$, DM annihilations to gg (via a box diagram) [96, 97] or three-body final states like tWb [96] can also contribute towards the relic density of the DM for a significantly large Yukawa coupling f_t. We do not consider these processes in our analysis as we found that these processes remain suppressed for the choice of f_t we are interested in for our analysis.

JHEP12(2022)167

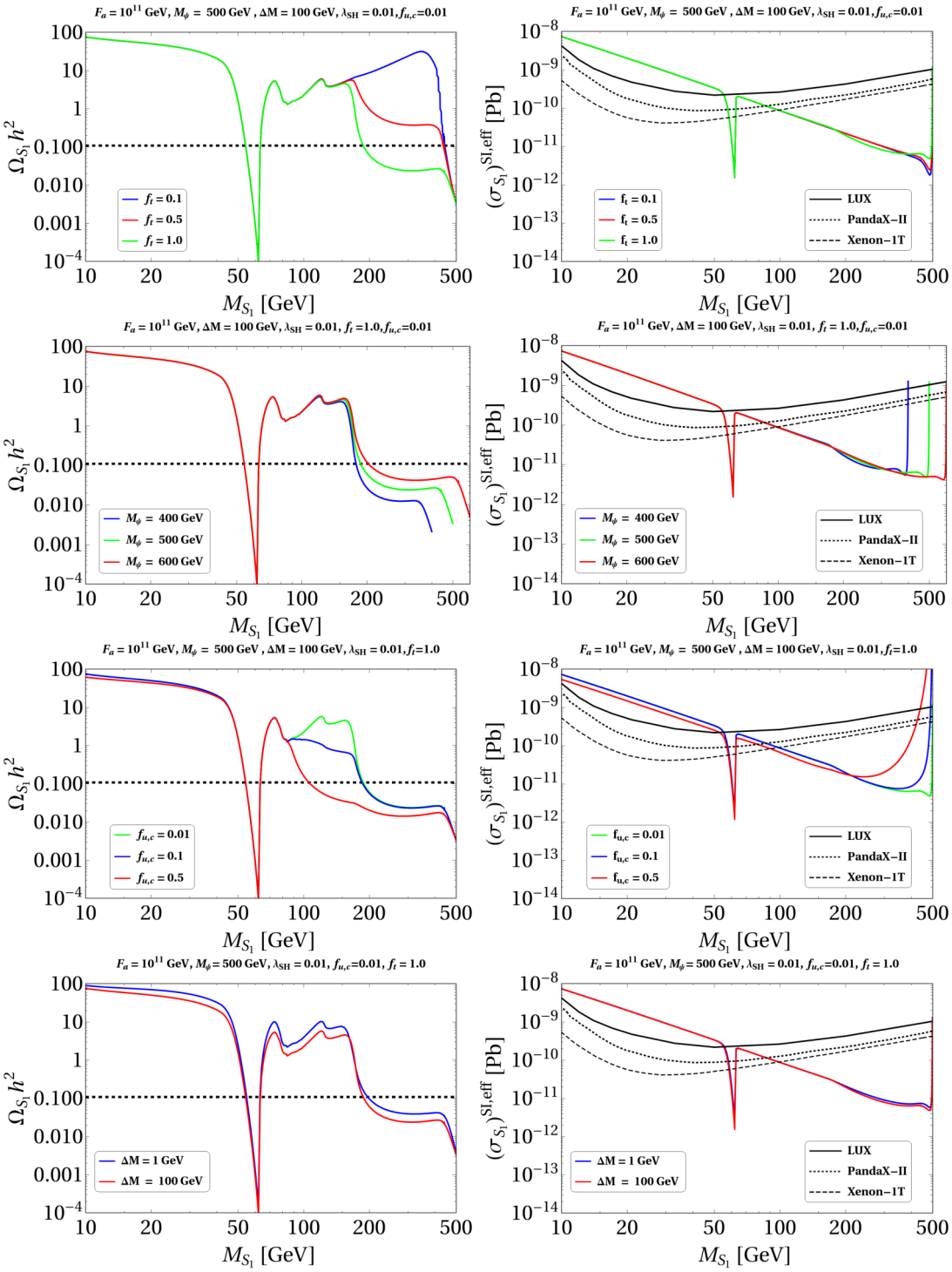

Figure 2. Variation of $\Omega_{S_1}h^2$ (left panel) and $\sigma^{\rm SI}_{S_{1,\rm eff}}$ (right panel) versus dark matter mass M_{S_1}. In all the plots we fix $F_a = 10^{11}$ GeV, $\lambda_{SH} = 0.01$. The Black dashed line in all the left plots corresponds to $0.120 - \Omega_a h^2$.

JHEP12(2022)167

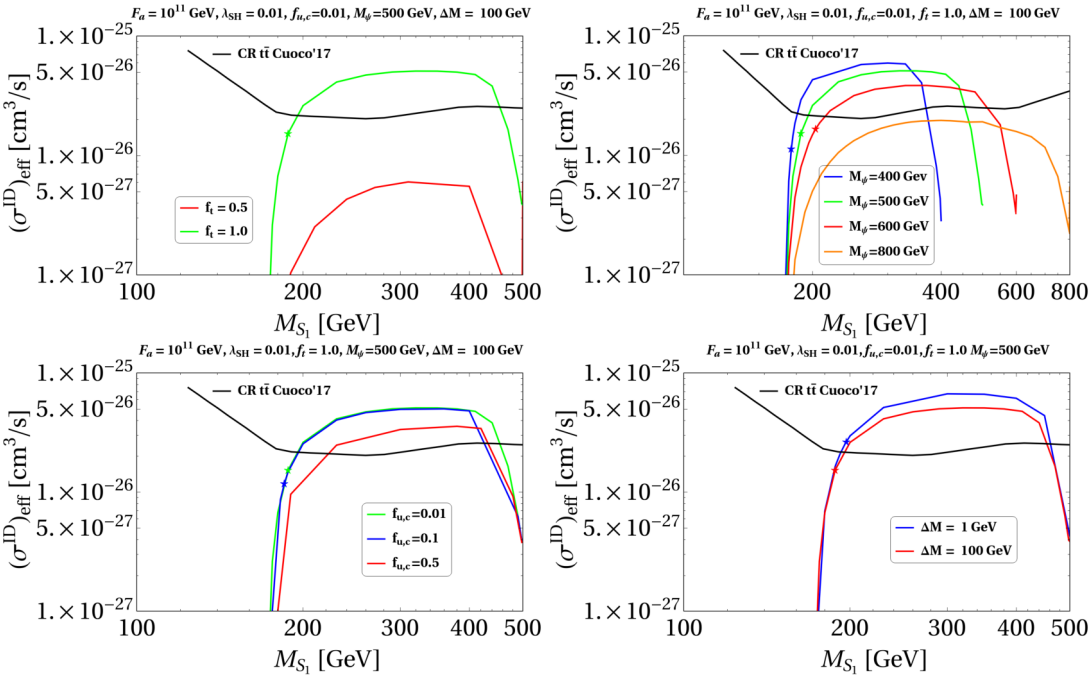

Figure 3. Variation of effective indirect detection cross-section versus DM mass. Variation for different values of f_t, the mass of VLQ, $f_{u,c}$, and ΔM are shown in top left, top right, bottom left and bottom right panels respectively. In all the plots we fix $F_a = 10^{11}$ GeV, $\lambda_{SH} = 0.01$. The solid black line shows the experimental upper bound in $t\bar{t}$ final state.

the DM co-annihilates with M_Ψ, the annihilation of Ψ with $\bar{\Psi}$ to the gluons dominates the effective annihilation cross-section (see eq. (4.4)) of the DM. Due to these co-annihilations, the relic density dark matter finally satisfies the condition $0.120 - \Omega_a h^2$ (denoted by the black dashed line) at $M_{S_1} = 444\,\text{GeV}$. Further increasing f_t to the higher values like 0.5 and 1.0, one notices that the DM annihilations to top quarks mediated by M_Ψ (see appendix A) start to dominate once the threshold of $M_{S_1} = M_{\text{top}}$ is crossed and the relic density can also satisfy the condition $0.120 - \Omega_a h^2$ near about $M_{S_1} \simeq 200\,\text{GeV}$ for $f_t = 1.0$. This figure illustrates the importance of VLQ in the DM phenomenology of the present setup as it makes huge parameter space allowed from the relic density, which was originally disallowed in the pure scalar singlet DM scenario.

In the top-right panel, we plot the spin-independent effective direct detection cross-section of S_1 with the DM mass and compare it with the experimental results. Notice that only the coupling f_u enters the direct detection cross-section of DM apart from the Higgs-portal coupling λ_{SH}. Note that the reduced values in the effective direct detection cross-section are the result of the rescaling in the two-component DM system (see eq. (4.8)). Additionally, Higgs resonance dip at $M_{S_1} = M_h/2$ and rise at $M_{S_1} \simeq 500\,\text{GeV}$ because of the interference among the direct detection diagrams (see appendix A). Here, one notices that the near resonance region remains discarded from the experimental bounds. Still, the other regions where relic density can be satisfied remain allowed from the direct detection searches.

JHEP12(2022)167

In the left panel of the second row in figure 2 we fix $f_t = 1.0$ and then study the effect of varying M_Ψ in $\Omega_{S_1}h^2 - M_{S_1}$ plane. As expected, the final fall in the relic density pattern happens at three different positions corresponding to the three different values of M_Ψ. With the heavier propagator mass i.e. $M_\Psi = 600\,\text{GeV}$, the effective annihilation cross-section of the DM to the top quark remains smaller in comparison to what is observed for $M_\Psi = 400\,\text{GeV}$ and hence relatively larger relic density is observed for $M_\Psi = 600\,\text{GeV}$ than for $M_\Psi = 400\,\text{GeV}$. Similarly, in the left panel of the third row, we depict the effect of varying f_u and f_c. For simplicity, here we also assume $f_u = f_c$. As expected, for a large value of $f_{u,c}$ the annihilation of DM to top and up (charm) quark final state also becomes dominant the moment the threshold $2M_{S_1} = M_{\text{top}} + M_{u(c)}$ is achieved. This leads to an increase in the DM annihilation cross-section, and consequently, a decrease in the relic density is observed. Next, in the left panel of the fourth row we show the effect of varying ΔM on the relic density of the DM. As expected, a smaller ΔM results in a larger effective DM annihilation cross-section and hence a smaller relic, so in order to satisfy the correct relic density a heavier DM mass is required. On the other hand, a larger ΔM requires a smaller DM mass to satisfy the observed relic density and hence the plot shifts towards the lower DM mass. Finally, the middle and bottom right panel of figure 2 can be followed from the one observed in the top right panel.

As can be seen from figure 2, the correct relic density is mostly satisfied in the parameter space where $M_{s_1} > M_t$. Hence, one needs to check the prospects of indirect detection of DM in our model specifically focusing on $t\bar{t}$ final states from the DM annihilations. We display our findings in figure 3 where we plot the effective indirect detection cross-section with DM mass and show the experimental upper bound (black solid line) of DM annihilating to $t\bar{t}$ final states that can be obtained from antiproton cosmic ray data [86]. In the top left panel of figure 3, we find that the DM mass for which the observed relic density satisfied (shown by green $\star$) in the top left panel of figure 2 is also allowed from the constraints coming from the indirect search bound. A similar situation is also observed in the top right and bottom left panels. On the other hand, in the bottom right panel where the variation with ΔM is studied, it found that a larger $\Delta M \sim 100\,\text{GeV}$ is prefered if one also considers the constraints coming from indirect search experiments. For this reason, we fix $\Delta M = 100\,\text{GeV}$ throughout our analysis.

In figure 4, we show the parameter space that remains consistent with the DM constraints and is also allowed by the constraints that come from the flavor observable like $D^0 - \bar{D}^0$ mixings in the bi-dimensional plane of $\Delta M_{\Psi S_1}/M_{S_1}$ Vs M_{S_1}, where $\Delta M_{\Psi S_1}$ is the mass difference between VLQ and DM, $M_\Psi - M_{S_1}$. Here, the dependence upon different Yukawa couplings ($f_u = f_c$ in the left panel and f_t in the right panel of the figure) is spotted with a continuous color map. Two discrete narrow slices at the top-left corner due to Higgs resonance. We are primarily interested in the non-resonant continuous region extended over vast parameter space. At the lower M_{S_1} end, this continuous region opens up when the DM pair annihilate into a top quark and up (charm) quark (see appendix A). Eventually, for a choice of heavier mass, the DM pair starts annihilating into the top pair.

This allowed region can be categorized into two distinct parts as upper and lower regions separated by a line where the mass difference between VLQ and DM equates to the top mass. Hence the upper region can be probed at the collider with on-shell production of

JHEP12(2022)167

Figure 4. Parameter space satisfying observed DM abundance and also allowed by the direct search experiments in the bi-dimensional plane of $\frac{\Delta M_{\Psi S_1}}{M_{S_1}} - M_{S_1}$, where the colour coding is done with respect to: Left Panel: the Yukawa couplings $f_u = f_c$ and Right Panel: the Yukawa coupling f_t. In both the plots we fix $F_a = 10^{11}$ GeV, $\lambda_{SH} = 0.01$, $\Delta M = 100\,\text{GeV}$ while we vary f_t in the range 0–1.5 and $f_u = f_c$ in the range 0–1.5.

top quark from VLQ decay, while the lower region is sensitive to a probe with light quark search. We will further demonstrate in the next section how top quark searches from the boosted top jet can improve the search strategy in this region.

As a consequence of the narrow mass gap between scalar DM and VLQ, co-annihilation takes a leading role in most parts of the lower region. Precisely because of the same reason, this region is also susceptible to the direct detection probe. Variations of color contours for different f_u values are evident in the lower region of the left plot in figure 4. This reflects the gradually larger parameter space excluded due to direct detection constrain for a choice of larger f_u values. The lower value of mediator mass increases the direct detection cross-section. In order to keep this cross-section below the current direct detection bounds, a smaller f_u is required. On the contrary, the direct search experiments allow the upper region irrespective of the choice of f_u, and hence a uniform distribution of the colors is observed. This is because even for a large f_u, the DM-nucleon scattering cross-section still remains small due to the presence of a heavier mediator *i.e* M_Ψ.

At the right part of the same plot, one finds that with an increasing DM mass, a relatively smaller $\Delta M_{\Psi S_1}/M_{S_1}$ is required in order to satisfy the correct relic density, while the interplay between the DM mass, mediator's mass and the f_u makes these points allowed from the direct detection constraints. In this region, the DM dominantly annihilates into the top-quark pair and sub-dominantly into the top quark and up (charm) quark final states. Next, in the right panel of figure 4, we show the color coding with respect to f_t in order to highlight its significance. One observes the correct relic density in the top-left region of the plot due to the involvement of a large f_t as is also evident from the top left panel of figure 2. As expected for a lighter mediator mass, a relatively smaller f_t is required to satisfy the correct relic density, as is also observed while moving downward in the plot. Finally, the role of f_t becomes more prominent once the $M_{S_1} = M_{\text{top}}$ threshold is opened, as can also be seen from the right side of the plot.

JHEP12(2022)167